Vol 10 No 12, December 2001
1009-1963/2001/10(12)/1157-06

Chinese Physics

© 2001 Chin. Phys. Soc.
and IOP Publishing Ltd

EFFECT OF α-Fe SURFACE LAYER ON THE MAGNETIC REVERSION PROCESS FOR $Nd_2Fe_{14}B$ CRYSTAL*

ZHAO SU-FEN(赵素芬), JIN HAN-MIN(金汉民),
WANG XUE-FENG(王学凤), and YAN YU(闫 羽)
Department of Physics, Jilin University, Changchun 130023, *China*

(Received 13 February 2001; revised manuscript received 10 July 2001)

The demagnetization process for a $Nd_2Fe_{14}B$ grain covered by an α-Fe layer was studied by use of the finite element technique of micromagnetics. $\mu_0{}_i H_c$ decreases with the increase of α-Fe layer thickness t. With the increase of t from 0 to 6nm, $\mu_0{}_i H_c$ decreases from ~7 T to ~3.5 T when the angle between the applied field and the c-axis of the $Nd_2Fe_{14}B$ grain is 0.5° and from ~4 T to ~1.5 T when the angle is 30° or 60°. The effect is only slightly affected by the angle between the α-Fe layer and the field direction.

Keywords: hysteresis loop, permanent magnet, micromagnetics
PACC: 7560E, 7550B, 7540M

I. INTRODUCTION

It is well established that a sintered Nd–Fe–B magnet is coated with an oxidized (α-Fe+Nd_2O_3) surface layer of a thickness of the order of ~10 nm,[1] and the partly oxidized surface $Nd_2Fe_{14}B$ grain has a considerably small coercive force $\mu_0{}_i H_c$ than that of the ensemble of the inner $Nd_2Fe_{14}B$ grains.[2] The demagnetization process of the partly oxidized $Nd_2Fe_{14}B$ grain, however, has not been studied in detail. In this paper we will analyse the demagnetization process and evolution of the spin distribution during the demagnetization process for the grain by using the finite element technique of micromagnetics.[3–4]

II. MODEL AND CALCULATIONS

The system considered is a cubic magnet of a volume $L \times L \times L$ (L=20nm) consisting of a $Nd_2Fe_{14}B$ grain of volume $L \times L \times (L-t)$ and an α-Fe surface layer of volume $L \times L \times t$. The polar angles of the c-axis of the $Nd_2Fe_{14}B$ grain are (θ_c,φ_c) in the xyz coordinate system where the x, y and z axes are parallel to the edges of the magnet, the $< 100 >$ axes of α-Fe are along the x, y and z axes, and the applied field $\boldsymbol{H}_{ap}$ is applied along the z-axis. The magnet is divided into $m \times m \times m$ (m=5) cubic regions, and each region is subdivided further into 24 tetrahedral elements, each of a volume $V_e = \frac{1}{24}\left(\frac{L}{m}\right)^3$. The four vertices of the tetrahedral element are located at the cubic centre (vertex 1), the centre of the surface (vertex 2), and two vertices of the surface of the cubic region (vertices 3 and 4), respectively (Fig.1).

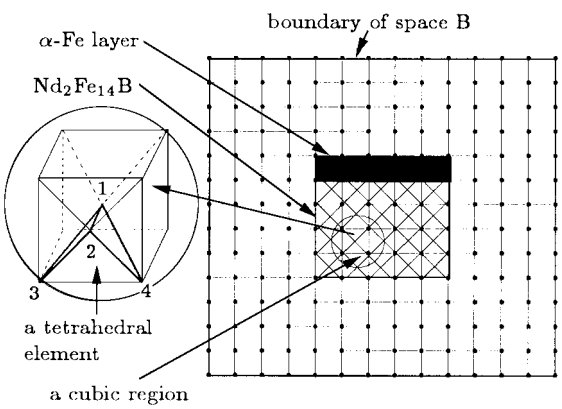


Fig.1. The magnet, cubic region, tetrahedral element and space B.

The total energy G of the system is comprised of the Zeeman energy F_H, the magnetocrystalline anisotropy energy F_K, the exchange energy F_X and the stray field energy F_M. To calculate F_H, F_X and the K_1 term of F_K for $Nd_2Fe_{14}B$, it is assumed approximately that the magnetic polarization vector $\boldsymbol{J}_s(\boldsymbol{r})$ in an element is a linear function of the position vector $\boldsymbol{r}$, that is

$$\boldsymbol{J}_s(\boldsymbol{r}) = \sum_{i=1,2,3,4} \eta_i \boldsymbol{J}_s(i), \qquad (1)$$

where

$$\eta_1 \equiv \frac{\boldsymbol{l}(2\boldsymbol{r}) \cdot (\boldsymbol{l}(24) \times \boldsymbol{l}(23))}{\boldsymbol{l}(21) \cdot (\boldsymbol{l}(24) \times \boldsymbol{l}(23))}, \eta_2 \equiv \frac{\boldsymbol{l}(4\boldsymbol{r}) \cdot (\boldsymbol{l}(41) \times \boldsymbol{l}(43))}{\boldsymbol{l}(42) \cdot (\boldsymbol{l}(41) \times \boldsymbol{l}(43))},$$

*Project supported by the National Natural Science Foundation of China (Grant No. 59871019).

$$\eta_3 \equiv \frac{\boldsymbol{l}(2\boldsymbol{r})\cdot(\boldsymbol{l}(21)\times\boldsymbol{l}(24))}{\boldsymbol{l}(23)\cdot(\boldsymbol{l}(21)\times\boldsymbol{l}(24))}, \eta_4 = 1-(\eta_1+\eta_2+\eta_3);$$

$\boldsymbol{J}_s(i)$ is $\boldsymbol{J}_s$ at the vertex i, and $\boldsymbol{l}(ij)$ and $\boldsymbol{l}(i\boldsymbol{r})$ are the space vectors from the vertex i to vertex j and to $\boldsymbol{r}$, respectively.

The energies for an element, therefore, are approximated by

$$F_H(\text{element}) = -\int_{\text{element}} \boldsymbol{H}_{ap}\cdot\boldsymbol{J}_s(\boldsymbol{r})dv \approx \frac{V_e\boldsymbol{H}_{ap}}{4}\cdot\sum_i^{1,2,3,4}\boldsymbol{J}(i), \tag{2}$$

$$\begin{aligned} F_X(\text{element}) =& A\int_{\text{element}}\sum_\gamma^{x,y,x}[\nabla\alpha_\gamma(\boldsymbol{r})]^2dv \approx \frac{A}{J_s^2}\int_{\text{element}}\sum_{i,j}^{1,2,3,4}[\boldsymbol{J}_s(i)\cdot\boldsymbol{J}_s(j)][\nabla\eta_i\cdot\nabla\eta_j]dv \\ =& -V_e\left(\frac{2m}{L}\right)^2\frac{A}{J_s^2}\boldsymbol{J}_s(2)\cdot[2\boldsymbol{J}_s(1)+\boldsymbol{J}_s(3)+\boldsymbol{J}_s(4)]+\text{const}, \end{aligned} \tag{3}$$

$$\begin{aligned} F_{K_1NdFeB}(\text{element}) =& \int_{\text{element } t} K_1\sin^2\theta_{<100>}(\boldsymbol{r})dv \approx \frac{K_1}{J_s^2}\int_{\text{element}}[J_s^2-\sum_{ij}^{1,2,3,4}(\boldsymbol{J}_s(i)\cdot\boldsymbol{e}_c)(\boldsymbol{J}_s(j)\cdot\boldsymbol{e}_c)]\eta_i\eta_j dv \\ =& -\frac{K_1V_e}{10J_s^2}\left[\sum_i^{1,2,3,4}(\boldsymbol{J}_s(i)\cdot e_c)^2+\sum_{i>j}^{1,2,3,4}(\boldsymbol{J}_s(i)\cdot\boldsymbol{e}_c)\boldsymbol{J}_s(j)\cdot e_c)\right]+\text{const}. \end{aligned} \tag{4}$$

Here, $\boldsymbol{e}_c$ is the unit vector along the c-axis, and $\theta_{<100>}$ is the angle between $\boldsymbol{J}_s$ and $\boldsymbol{e}_c$. The densities of other energy terms in an element are approximated as a linear function of $\boldsymbol{r}$, such that the K_2 term in F_K for $Nd_2Fe_{14}B$ and F_K for α-Fe are respectively

$$\begin{aligned} F_{K_2NdFeB}(\text{element}) =& \int_{\text{element}} K_2\sin^4\theta_{<100>}(\boldsymbol{r})dv \\ \approx& \frac{K_2V_e}{4}\sum_i^{1,2,3,4}\sin^4\theta_{<100>}(i), \end{aligned} \tag{5}$$

$$\begin{aligned} F_{KFe}(\text{element}) =& \int_{\text{element}}\Big[K_1\sum_{\gamma\delta}^{xy,yz,zx}\alpha_\gamma^2(\boldsymbol{r})\alpha_\delta^2(\boldsymbol{r}) \\ &+K_2\alpha_x^2(\boldsymbol{r})\alpha_y^2(\boldsymbol{r})\alpha_z^2(\boldsymbol{r})\Big]dv \\ \approx& \frac{V_e}{4}\sum_i^{1,2,3,4}\Big[K_1\sum_{\gamma\delta}^{xy,yz,zx}\alpha_\gamma^2(i)\alpha_\delta^2(i) \\ &+K_2\alpha_x^2(i)\alpha_y^2(i)\alpha_z^2(i)\Big]. \end{aligned} \tag{6}$$

Here $\alpha_\gamma(\gamma = x,y,z)$ are the direction cosines of $\boldsymbol{J}_s$. F_M is replaced by the following function F_W,[5]

$$F_W = \frac{1}{2\mu_0}\int_B[\nabla\times\boldsymbol{A}(\boldsymbol{r})-\boldsymbol{J}_s(\boldsymbol{r})]^2dv. \tag{7}$$

The integration runs over the cubic space B of dimension $\left[L(1+2\frac{4}{m})\right]^3$, which symmetrically surrounds the magnet. To calculate F_W approximately, the tetrahedral element division used in the magnet is extended to the whole space of B (Fig.1). The partial differential of $\frac{\partial A_\beta}{\partial\gamma}(\beta,\gamma=x,y,z)$ is approximated by the ratio of the finite differences ΔA_β to $\Delta\gamma$ between the nearest-neighbour grid points.[6] The function $[\nabla\times\boldsymbol{A}(\boldsymbol{r})-\boldsymbol{J}_s(\boldsymbol{r})]^2_\gamma$ in an element is treated as a linear function of $\boldsymbol{r}$.

The applied field H_{ap} is decreased from 5 T by steps, and the polarization J for the magnet under each H_{ap} is obtained from minimizing the energy G with respect to the polar angles of $\boldsymbol{J}_s(i)$, $\{\theta(i),\varphi(i)\}$, at the vertices of the tetrahedral elements in the magnet and the components of $\boldsymbol{A}(i)$, $\{A_x(i),A_y(i),A_z(i)\}$, at the grid points within the space B under the boundary conditions of $\boldsymbol{A}(j)=\left(\frac{L}{m}\right)^3\sum_k^{m^3}\frac{\boldsymbol{J}_s(k)\times\boldsymbol{r}_{kj}}{4\pi r_{kj}^3}$ at the grid points j on the boundary faces of space B. Here $\boldsymbol{A}(j)$ is the magnetic vector potential, $\boldsymbol{J}_s(k)$ the $\boldsymbol{J}_s$ at the centre of cubic region k, and $\boldsymbol{r}_{kj}$ the space vector from the centre of the cubic region k to the grid point j. Under the minimum condition, F_W becomes F_M and $\boldsymbol{A}$ in Eq.(7) the magnetic vector potential.[5]

The following values of magnetic constants at room temperature are used in the calculations[7]: J_s=1.63T, A=7.7×10^{-12}J/m, K_1=4.3×10^{6}J/m^3 and K_2=0.65×10^{6}J/m^3 for $Nd_2Fe_{14}B$, and J_s=2.15T, A=2.5×10^{-11}J/m, K_1=4.6×10^{4}J/m^3 and K_2=1.50×10^{4}J/m^3 for α-Fe. The minimization of energy is obtained by using the conjugate gradient method.[8]

Ⅲ. RESULTS AND DISCUSSION

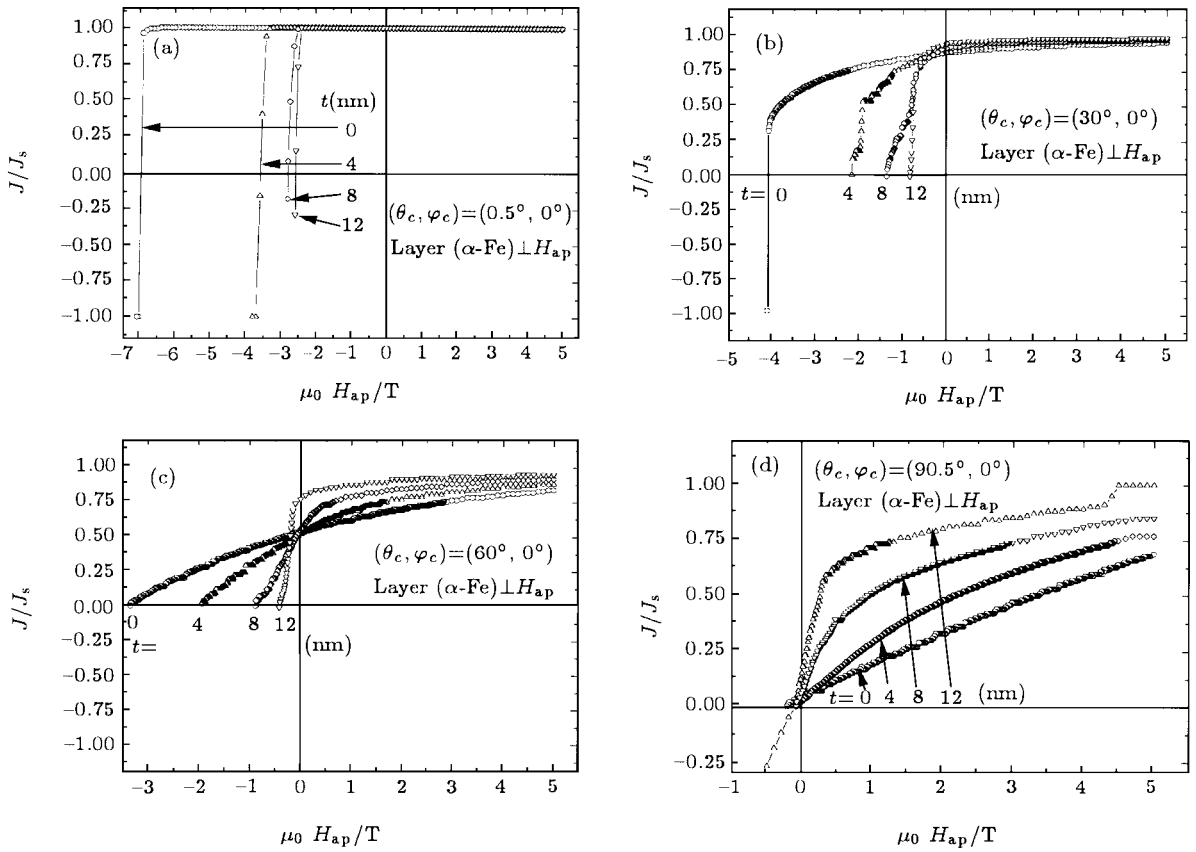


Fig.2. The demagnetization curves for the α-Fe layer vertical to H_{ap}: (θ_c, φ_c)=(0.5,0) degrees (a), (30,0) degrees (b), (60,0) degrees (c) and (90.5,0) degrees (d) with thickness t=0, 4, 8 and 12 nm.

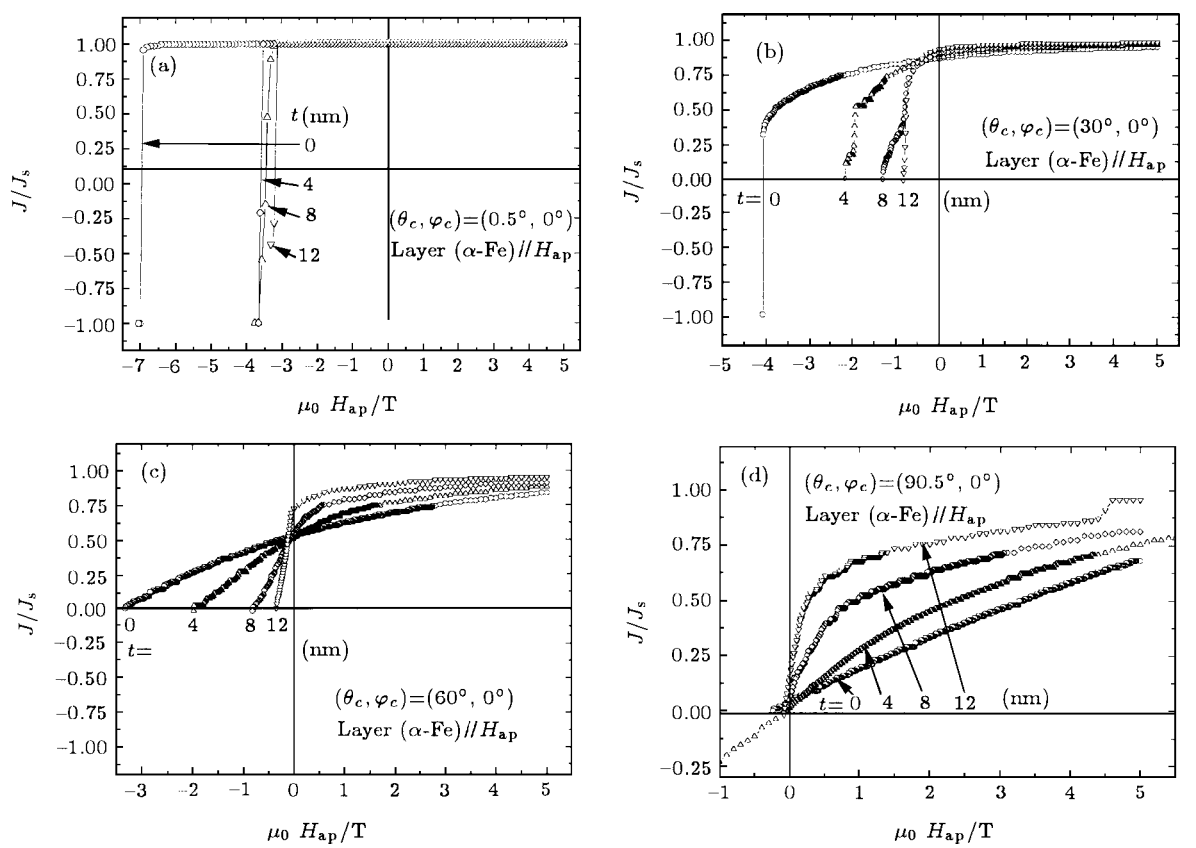


Fig.3. The demagnetization curves for the α-Fe layer parallel to H_{ap}: (θ_c, φ_c)=(0.5, 0) degrees (a), (30,0) degrees (b), (60,0) degrees (c) and (90.5,0) degrees (d) with thickness t=0, 4, 8 and 12nm.

Figures 2 and 3 show the demagnetization curves for the α-Fe layer vertical (Fig.2) and parallel (Fig.3) to $\boldsymbol{H}_{\rm ap}$, respectively, with thickness t=0, 4, 8 and 12 nm. Figures 2(a)–2(d) are for $(\theta_{\rm c}, \varphi_{\rm c})$=(0.5, 0), (30,0), (60,0) and (90.5,0) degrees, respectively.

Figure 4 summarizes the t dependence of $\mu_{0\,\rm i}H_{\rm c}$. With the increase of t, $\mu_{0\,\rm i}H_{\rm c}$ and its slope decrease; $\mu_{0\,\rm i}H_{\rm c}$ decreases by about one half when t increases from 0 to 4 nm, and by about three quarters when t is increased to 12 nm for $\theta_{\rm c}$=30~60°. The demagnetization curve is only slightly affected by the α-Fe layer orientation.

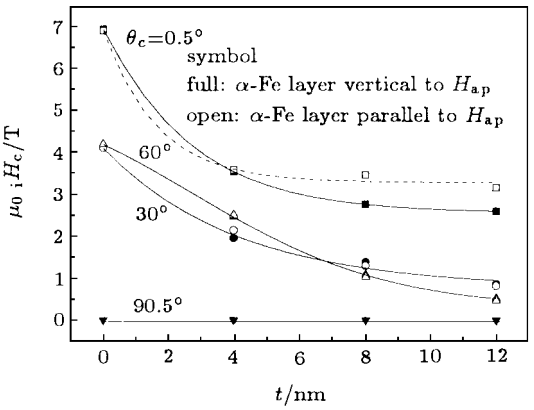


Fig.4. t dependence of $\mu_{0\,\rm i}H_{\rm c}$.

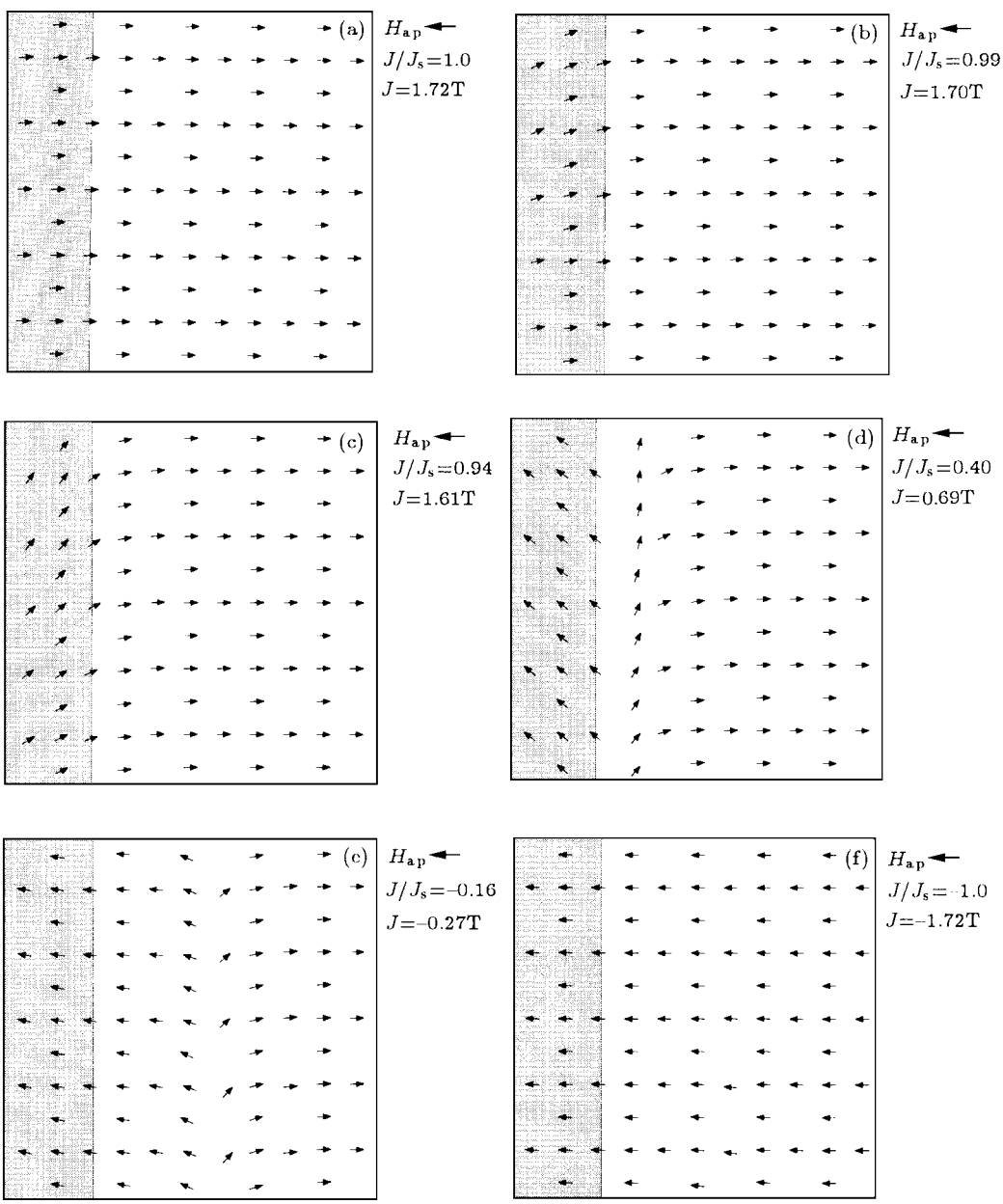


Fig.5. The spin distribution at $\mu_0 H_{\rm ap}$=–3.2 (a), –3.3 (b), –3.4 (c), –3.5 (d), –3.55 (e) and –3.65T (f). The α-Fe layer (shaded area) is vertical to $H_{\rm ap}$, t=4 nm and $(\theta_{\rm c}, \varphi_{\rm c})$=(0.5, 0) degrees.

Figure 5 shows the spin distribution on a cross section parallel to the yz plane, including the vertices 1 and 2, during the demagnetization for (θ_c, φ_c)=(0.5, 0), t=4nm, when the α-Fe layer is vertical to the z-axis.

When $\boldsymbol{J}_s$ starts to deviate from the z-axis this is observed in the α-Fe layer at $\mu_{0\,i}H_{ap}$=–3.3 T, which is much smaller than the negative anisotropic field of α-Fe, $-\mu_0\dfrac{2K_1}{J_s} \approx -0.05$T (Fig.5(b)). An irreversible rotation occurs in the α-Fe layer at $\mu_{0\,i}H_{ap}$=–3.5T by forming a 180° domain wall along the α-Fe—$Nd_2Fe_{14}B$ boundary (Fig.5(d)). Then, the reversed domain expands into the $Nd_2Fe_{14}B$ grain, and the domain wall pinning appears within the $Nd_2Fe_{14}B$ grain at a field of $\mu_{0\,i}H_{ap}$=–3.55T (Fig.5(e)). The pinning is caused by the decrease of the stray field along the negative z-direction at the wall with the movement of the wall, which sweeps the whole $Nd_2Fe_{14}B$ grain at $\mu_0\boldsymbol{H}_{ap} \geq -3.6$T (Fig.5(f)).

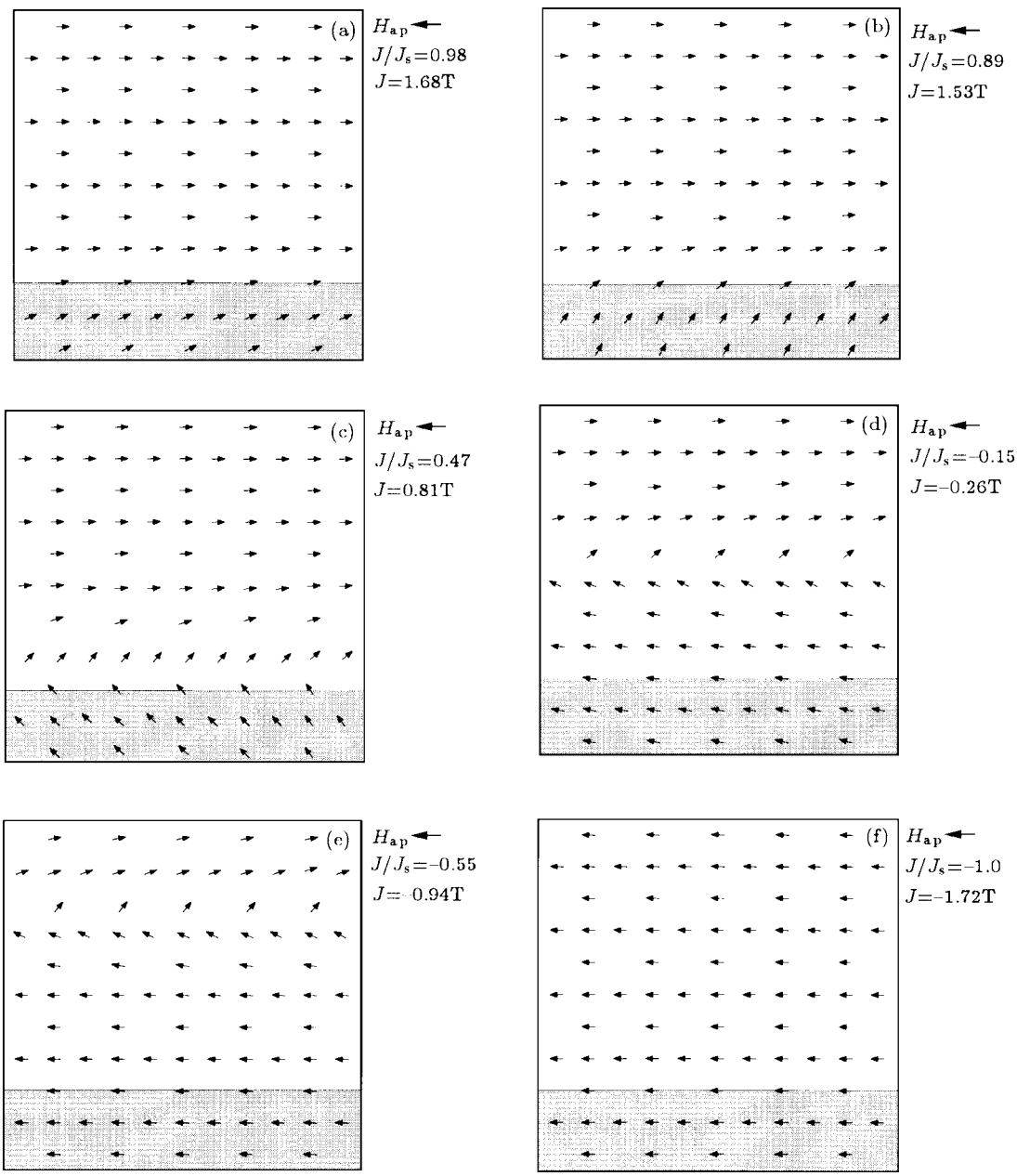


Fig.6. The spin distribution at $\mu_0 H_{ap}$=–3.2 (a), –3.3 (b), –3.4 (c), –3.45 (d), –3.55 (e) and –3.65 T (f). The α-Fe layer (shaded area) is parallel to the z-axis, t=4 nm and (θ_c, φ_c)=(0.5, 0) degrees.

Figure 6 is the counterpart of Fig.5 for α-Fe layer parallel to $\boldsymbol{H}_{\rm ap}$. The deviation of $\boldsymbol{J}_{\rm s}$ from the z-axis in the α-Fe layer begins earlier than for the α-Fe layer vertical to $\boldsymbol{H}_{\rm ap}$ because the stray field from the $Nd_2Fe_{14}B$ grain is no longer positive as corresponds to Fig.5, but now it is negative (Fig.6(a)). The irreversible rotation occurs in the α-Fe layer at $\mu_{0\,\rm i}H_{\rm ap}$=–3.4T by forming an 180° domain wall along the α-Fe—$Nd_2Fe_{14}B$ boundary (Fig.6(c)). The reversed domain expands into the $Nd_2Fe_{14}B$ grain and the wall is also pinned within the $Nd_2Fe_{14}B$ grain in the field around $\mu_{0\,\rm i}H_{\rm ap}$=–3.45T (Fig.6(d)). The pinning results from the decrease of the stray field along the negative z-direction in the wall as the latter moves. The wall sweeps the whole $Nd_2Fe_{14}B$ grain at $\mu_{0\,\rm i}H_{\rm ap}$=–3.6T.

In conclusion, the α-Fe layer playing the role of nucleation centre of the reversed domain diminishes the coercive force of the magnet sharply. But the result cannot explain the much smaller coercive force observed on the surface grains for the multi-grain Nd–Fe–B magnet. In the latter case, each part of the α-Fe layer on different grains are exchange coupled with the neighbouring α-Fe layer parts, and the demagnetization process is expected to be more complicated. A study of the effect of the α-Fe layer on the demagnetization process for the multi-grain Nd–Fe–B magnet is underway.

References

[1] Blank R and Adler E 1987 *Proc. 9th Int. Workshop on RE magnets* p 537

[2] Pastushenkov Yu G, Afamasieva L E and Grechishkin R M 1994 *Phys. Status Solidi* a **142** K41

[3] Wang X F, Jin H M, Zhao S F and Yan Y 2001 *Chin. Phys.* **10** 555

[4] Jin H M, Wang X F, Zhao S F and Yan Y 2001 *Chin. Phys.* **10** 862

[5] Asselin P and Thiele A A 1986 *IEEE Trans. Magn.* **22** 1876

[6] Jin H M, Kim Y B and Wang X F 1998 *J. Phys.: Condens. Matter* **10** 7243

[7] Fischer R, Schrefe T, Kronmüller and Fidler J 1996 *J. Magn. Magn. Mater.* **153** 35

[8] Gill P, Murray W and Wright M H 1981 *Practical Optimization* (London: Academic)